

Small Terminase Couples Viral DNA Binding to Genome-Packaging ATPase Activity

Ankoo Roy,¹ Anshul Bhardwaj,¹ Pinaki Datta,¹ Gabriel C. Lander,² and Gino Cingolani^{1,*}

¹Department of Biochemistry and Molecular Biology, Thomas Jefferson University, 233 South 10th Street, Philadelphia, PA 19107, USA

²Life Science Division, Lawrence Berkeley National Lab, 1 Cyclotron Road, Berkeley, CA 94720, USA

*Correspondence: gino.cingolani@jefferson.edu

<http://dx.doi.org/10.1016/j.str.2012.05.014>

SUMMARY

Packaging of viral genomes into empty procapsids is powered by a large DNA-packaging motor. In most viruses, this machine is composed of a large (L) and a small (S) terminase subunit complexed with a dodecamer of portal protein. Here we describe the 1.75 Å crystal structure of the bacteriophage P22 S-terminase in a nonameric conformation. The structure presents a central channel ~23 Å in diameter, sufficiently large to accommodate hydrated B-DNA. The last 23 residues of S-terminase are essential for binding to DNA and assembly to L-terminase. Upon binding to its own DNA, S-terminase functions as a specific activator of L-terminase ATPase activity. The DNA-dependent stimulation of ATPase activity thus rationalizes the exclusive specificity of genome-packaging motors for viral DNA in the crowd of host DNA, ensuring fidelity of packaging and avoiding wasteful ATP hydrolysis. This posits a model for DNA-dependent activation of genome-packaging motors of general interest in virology.

INTRODUCTION

Viral genome packaging is a complex, nonspontaneous reaction, catalyzed in many DNA viruses by a powerful genome-packaging motor (Casjens, 2011; Catalano, 2005; Rao and Feiss, 2008; Sun et al., 2010). This molecular machine consists of a dodecameric portal protein and an ATPase known as terminase that converts ATP hydrolysis into linear translation of DNA. In double-stranded DNA (dsDNA) bacteriophages, the terminase is formed by a small and a large subunit (referred to as S- and L-terminase), assembled in a complex of unknown stoichiometry. The ATPase activity resides in the L-terminase subunit, which binds directly to the portal protein (Rao and Feiss, 2008). In contrast, the S-terminase subunit binds to packaging initiation sites (referred to as *pac* in P22; Jackson et al., 1978) to prepare for genome packaging (Casjens et al., 1992) and regulates the ATPase activity of L-terminase (Baumann and Black, 2003; Leffers and Rao, 2000). This function is likely very important in vivo to sustain the enormous rate of genome-packaging, which can be as high as ~2,000 bp/sec (Fuller et al., 2007).

All S-terminases characterized to date adopt an oligomeric quaternary structure (Rao and Feiss, 2008), but the exact stoichiometry of assembly varies in different viruses. In bacteriophage P22, S-terminase (gp3) consists of 162 amino acids (molecular weight, ~18.6 kDa) and self-assembles into a nonameric ring (Nemecek et al., 2007; Nemecek et al., 2008; Roy et al., 2011). In contrast, the S-terminase subunit of bacteriophage Sf6, a close relative of P22 assembles into octamers (Zhao et al., 2010). Although octamers were also observed in solution for bacteriophage T7 (gp18) (White and Richardson, 1987) and T4 (gp16) (Lin et al., 1997) S-terminases, a recent crystal structure of the T4-like phage 44RR S-terminase (gp16) revealed a mix of undecamers and dodecamers (Sun et al., 2012). Similarly, phage SPP1 S-terminase (gp1) was reported to form decameric rings in solution (Camacho et al., 2003), but the crystal structure of the SPP1-like Bacillus phage SF6 revealed a mix of nonamers and decamers, with the nonamer being the predominant conformation (Büttner et al., 2012). Finally, phage λ S-terminase (gpNu1) forms a hetero-trimer bound to a monomer of L-terminase (gpA1), and in vitro this protomer can further assemble into tetramers (Maluf et al., 2006). Thus, as previously observed for viral portal proteins (Cingolani et al., 2002; Lorenzen et al., 2008), S-terminases appear to be highly polymorphic in solution and in crystal.

Similar to S-terminases, L-terminases can also oligomerize: a pentameric quaternary structure was suggested for T4 L-terminase bound to procapsid (Sun et al., 2008). The N-terminal ATPase domain of L-terminase is thought to contact directly the portal vertex (Sun et al., 2008), while the C terminus harbors a nuclease domain required to cleave DNA after encapsidation (Duffy and Feiss, 2002; Kanamaru et al., 2004). Regardless of the exact stoichiometry of assembly, the genes encoding L- and S-terminase subunits are essential in all tailed bacteriophages and herpesviruses (Rao and Feiss, 2008), underscoring their essential function in DNA packaging. Unfortunately, the molecular characterization of viral genome-packaging motors is in its infancy as compared to other multisubunit ATPases like the F₁-ATPase. Atomic-level structural information is presently available only for the full length L-terminase of T4 (Sun et al., 2008; Sun et al., 2007), and isolated L-terminase nuclease domains of SPP1 (Smits et al., 2009), P22 (Roy and Cingolani, 2012) and human cytomegalovirus (herpesvirus 5) (Nadal et al., 2010). No high-resolution information exists for the terminase holoenzyme or in complex with portal protein. Likewise, it is unclear how L- and S-terminase assemble during packaging to form a functional holoenzyme and how DNA is recruited to initiate packaging.

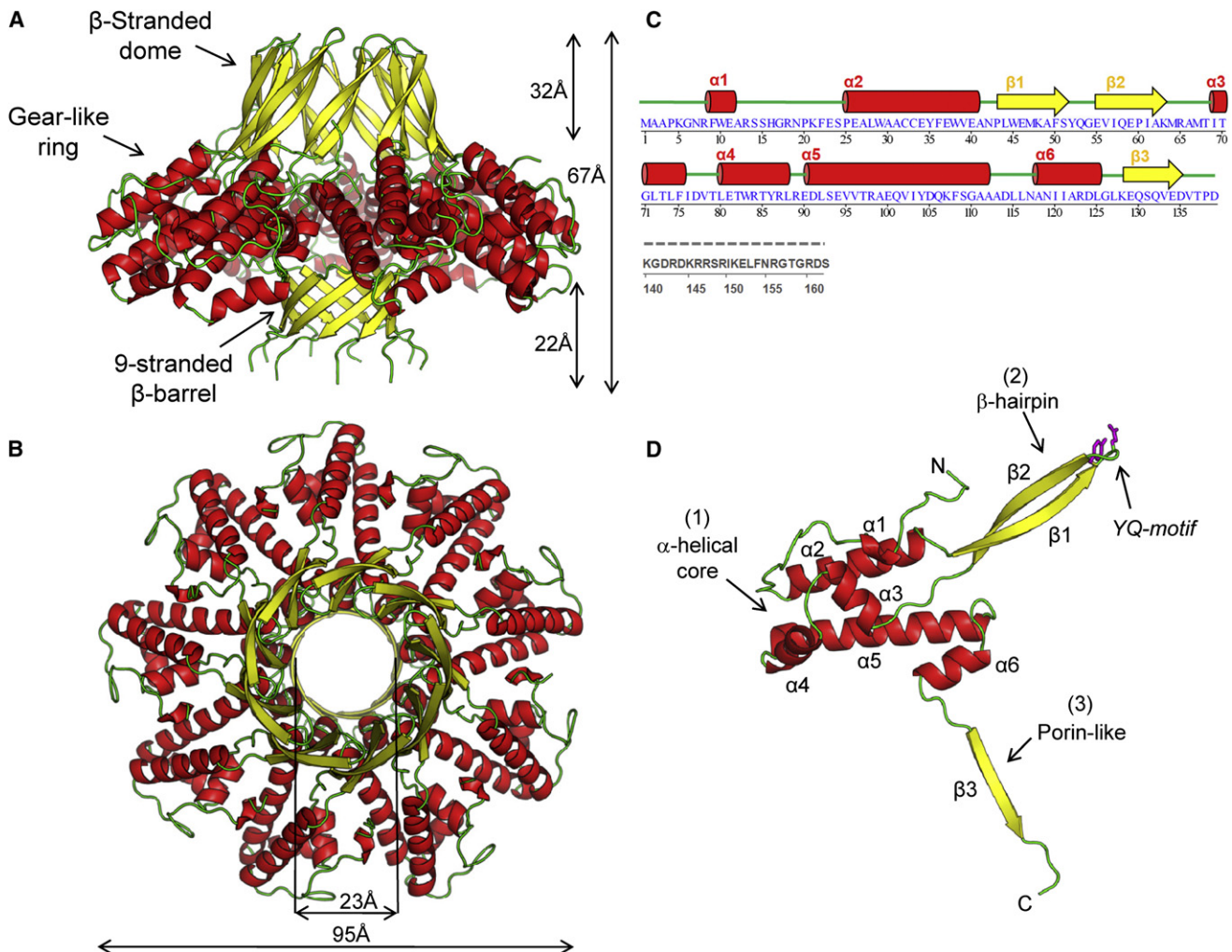


Figure 1. Quaternary Structure of the Nonameric S-Terminase Subunit of Bacteriophage P22

(A and B) Ribbon diagram of S-terminase in side (A) and top (B) views. The oligomer is colored by secondary structure elements with α helices, β strands and loops in red, yellow, and green, respectively. The overall diameter of S-terminase is ~ 95 Å with an internal hollow channel ~ 23 Å.

(C) Secondary structure and amino acid sequence of bacteriophage P22 S-terminase subunit. Dashed in gray is the DNA-binding domain spanning residues 140–162, which is proteolytically cleaved in the 1.75 Å structure used for high resolution refinement and is disordered in the 3.35 Å structure of fl-S-terminase (Figure S1B). The illustration was generated using STRIDE (Heinig and Frishman, 2004).

(D) Ribbon diagram of S-terminase protomer colored as in (A). The side chains for the YQ-motif on the tip of S-terminase are shown as sticks.

We have studied the S-terminase subunit of bacteriophage P22 to provide an atomic description of a prototypical S-terminase subunit and to determine its functional role in viral DNA packaging. Our results indicate that this protein is a dedicated, DNA-dependent ATPase-activating factor within the genome-packaging motor.

RESULTS

Structure Determination of the Bacteriophage P22 S-Terminase Subunit

The S-terminase subunit of bacteriophage P22 assembles in solution (Nemecek et al., 2007) into a homo-nonamer. In vitro, this oligomer unfolds irreversibly and in a highly cooperative manner, with an apparent melting temperature (T_m) of $\sim 85^\circ\text{C}$

(Figure S1A available online). We crystallized the full-length S-terminase in different space groups with one or two nonamers in the asymmetric unit (Roy et al., 2011). Although most crystals diffracted weakly to ~ 3.5 Å resolution, we found that omitting protease inhibitors during crystallization resulted in degradation of the last 23 C-terminal residues, which dramatically improved diffraction quality (Roy et al., 2011). We determined the crystal structure of P22 nonameric cleaved S-terminase to an $R_{\text{free}} \sim 21.65\%$, at 1.75 Å resolution (Figures 1A and 1B; Table 1). The entire polypeptide chain, with the exception of C-terminal residues 140–162, which are not present in the cleaved crystal form, has been unambiguously traced. This structural model was then used to phase an orthorhombic crystal form of full-length S-terminase grown in the presence of protease inhibitors (Table 1). Unexpectedly, this structure also had no discernible

Table 1. Crystallographic Data Collection and Refinement Statistics

	Cleaved S-Terminase		Full-Length S-Terminase
	Native-gp3	SeMet-gp3	FL-gp3
Data collection			
Space group	P2 ₁	P2 ₁	P2 ₁ 2 ₁ 2
Cell dimensions			
a, b, c (Å)	76.48, 100.90, 89.95	80.22, 101.18, 89.09	143.46, 144.93, 144.61
α, β, γ (°)	90, 93.73, 90	90, 92.87, 90	90, 90, 90
Wavelength (Å)	0.99	0.97	0.97
Resolution (Å)	15-1.75 (1.81-1.75)	20-2.5 (2.54-2.50)	20-3.35 (3.42-3.35)
Reflections (tot/unique)	2,483,158/ 126,076	7,505,096/ 49,292	747,842/43,496
R _{sym} ^a	7.1 (67.4)	9.6 (30.8)	17.5 (64.6)
I/σI	28.2 (1.8)	36.8 (9.0)	14.7 (3.3)
Completeness (%)	93.5 (62.5)	99.8 (100.0)	99.9 (99.7)
Redundancy	4.4 (3.3)	8.3 (8.1)	5.7 (5.6)
Refinement			
Resolution (Å)	15-1.75		20-3.35
No. reflections	126,076		41,398
R _{work} /R _{free} ^b	17.73/21.65		23.24/26.45
No. atoms			
Protein	11,158		19,348
Water	1,397		0
B-factors (Å²)			
Protein	36.5		59
Water	40.1		
r.m.s. deviations			
Bond lengths (Å)	0.006		0.009
Bond angles (°)	0.918		1.208

Values in parentheses are for highest-resolution shells.

^aR_{sym} = $\sum_{i,h} |I(i,h) - \langle I(h) \rangle| / \sum_{i,h} I(i,h)$ where I(i,h) and $\langle I(h) \rangle$ are the ith and mean measurement of intensity of reflection h.

^bThe R_{free} value was calculated using 2,000 reflections selected randomly for native-gp3 and in thin resolution shells for full-length S-terminase.

electron density for the last 23 residues, which, although present in crystal, are disordered in the crystal structure (Figures S1B and S1C).

P22 S-Terminase Folds into a Nonamer

The S-terminase subunit of bacteriophage P22 folds into a hollow nonameric ring of mixed α/β structure that resembles a jellyfish (Figures 1A and 1B). The quaternary structure of S-terminase consists of a central gear-like ring ~95 Å in diameter, which is sandwiched by a nine-stranded β-barrel, similar to that found in β-porins (Galdiero et al., 2007) and a β stranded dome, formed by nine slightly twisted β-hairpins (Figure 1A). The solvent-filled channel inside S-terminase varies between 20 Å and 25 Å in diameter (Figure 1B), large enough to accommodate B-DNA, which is ~20 Å in diameter in its hydrated form (Vlieghe et al., 1999). The nonamer is built by nine slightly nonidentical subunits,

symmetrically arranged around a central channel that has an overall height of ~67 Å (Figures 1A and 1B). Superimposition of S-terminase protomers reveals significant structural plasticity in the nine β-hairpins forming the β-dome (residues 42–65) that are rotated up ~8° with respect to each other. The body of each protomer is nearly parallel to the 9-fold axis running along the central channel (Figure 1A). The ring-shaped nonamer has a total solvent-accessible surface area of ~54,030 Å² and ~1,980 Å² of surface area is buried at the interface between two neighboring protomers. This interface is stabilized by a complex network of salt bridges between a largely positive face of one S-terminase protomer and the complementary largely negative face of its adjacent neighbor. Most notably, two inter-subunit salt bridges are observed between the amine nitrogen (Nz) atom and Ne atom of Arg8/Arg123 of one subunit and the Oε1 and Oε2 atoms of Glu40/Glu129 in the neighboring subunits. These ionic interactions may explain the salt dependency of ring formation observed in solution (Roy et al., 2011).

The structure of a single S-terminase protomer can be divided into four distinct domains (Figures 1C and 1D): (1) an N-terminal α-helical core formed by 6 α helices (α₁–α₆), which builds most of the gear-like ring, (2) a long β-hairpin (β₁–β₂), extending from the loop connecting helices α₂–α₃ (residues 41–69), which exposes at its tip a Tyr/Gln (YQ) motif, (3) a porin-like β strand (residues 126–139) that forms with its neighbors the nine-stranded β-barrel. To our knowledge, this is the first observed β-barrel in a soluble protein with more than eight strands (Galdiero et al., 2007), and (4) residues 140–162 are not present in the crystal form used for high-resolution refinement due to proteolytic cleavage in the crystallization drop (Roy et al., 2011). The same moiety has no discernable electron density in crystals of full-length S-terminase grown in the presence of PMSF (Figure S1C).

Structural Diversity of Viral S-Terminases

At least one S-terminase structure is available for each of the three families of tailed bacteriophages, which include *Podoviridae*, *Siphoviridae*, and *Myoviridae* (Ackermann, 2003). This structural repertoire provides a unique opportunity to identify similarities even in the absence of significant sequence conservation. For instance, despite only 15% sequence identity, the structure of P22 S-terminase presented in this paper shares an overall similar organization as the octameric S-terminase of bacteriophage Sf6 (Zhao et al., 2010). *Podoviridae* P22 (Figures 2A and 2B) and Sf6 (Figures 2C and 2D) S-terminases have equal height (~66 Å) and comparable diameter (~99 versus 95 Å), but differ in oligomerization state. Moreover, in P22 the internal channel is large enough throughout its length to accommodate hydrated dsDNA, while in Sf6 the channel diameter is ~27 Å in the helical core and narrows at the C-terminal end of the protein to ~17 Å, which, in the conformation observed crystallographically, is too narrow to accommodate dsDNA (Zhao et al., 2010). Superimposition of P22 and Sf6 protomers (Figure S2A) reveals structural similarity in five (helices α₂–α₆) of the six helices forming the α-helical core, while helix α₁ is not visible in the Sf6 model. The most noticeable difference between these two structures is that the long β-hairpin forming the β-stranded dome (residues 44–63) in P22 is missing in the Sf6 S-terminase (Figure S2A). Furthermore, the C-terminal domain of both

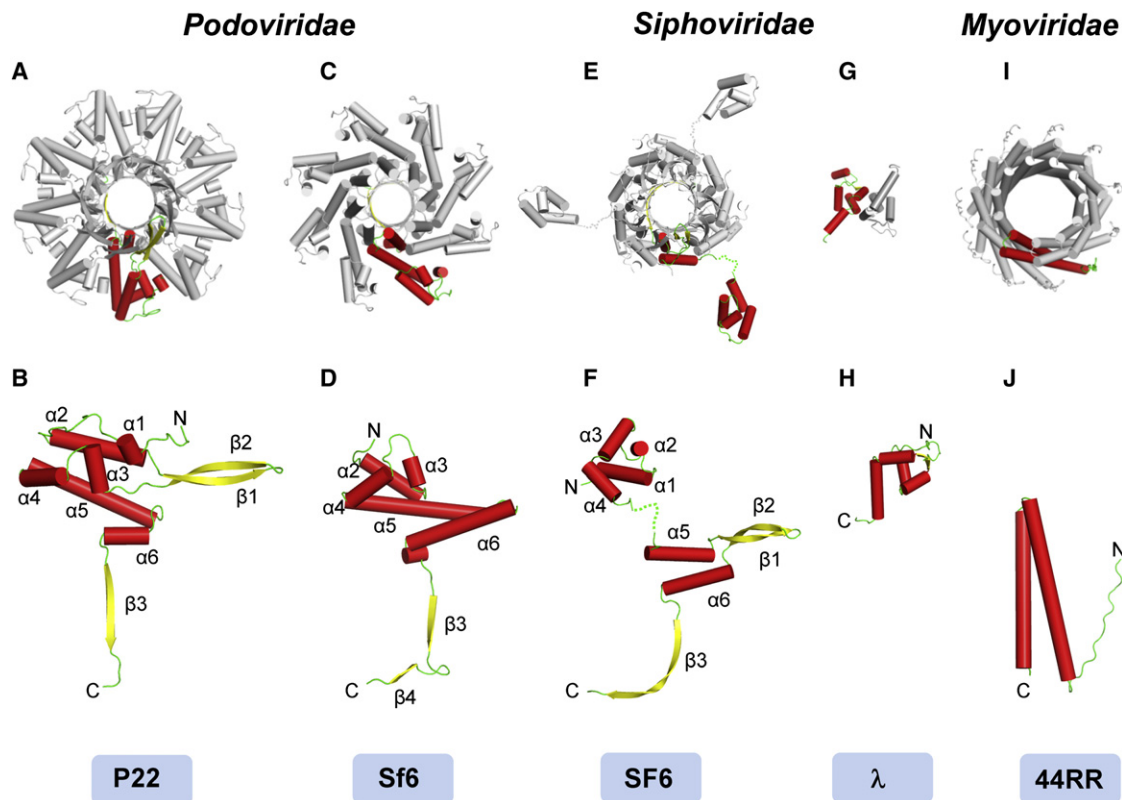


Figure 2. Conservation of S-Terminase in Tailed Bacteriophages

Oligomer and protomer structure of S-terminase subunits in Podoviridae P22 (A, B) and Sf6 (C, D) (PDB 3HEF); Siphoviridae SF6 (E and F) (PDB 3ZQQ) and λ (G and H) (PDB 1J9I); Myoviridae T4-like phage 44RR (I and J) (PDB 3TXQ). In all cases, the S-terminase is displayed from the top with α helices represented as cylinders; only one protomer per oligomer is colored by secondary structure elements, while the other subunits are in gray. Numbering of secondary structure elements in panels (B), (D), (F), (H), and (J) is relative to P22 S-terminase. See also Figure S2.

terminases folds into a porin-like barrel, but while in Sf6 a second β sheet follows strand β_3 , in P22 residues 140–162 downstream of strand β_3 are unstructured.

Partial structures of S-terminase subunits are also available for the SPP1-like *Bacillus* phage SF6 and λ , two members of the Siphoviridae family. SF6 (Figures 2E and 2F) (Büttner et al., 2012) and P22 (Figures 2A and 2B) S-terminases share a nonameric quaternary structure and a similar organization of the β -stranded dome and nine-stranded porin-like channel (Figure 1A), which are superimposable (rmsd ~ 2.2 Å). However, the β -hairpin β_1 – β_2 (forming the β -dome) originates at a topologically different position in the two terminases. In P22, it extends the loop between α helices α_2 – α_3 in the α -helical core (Figure 2B), while in SF6, it projects from helices α_5 – α_6 that form the oligomerization core (Figure 2F). Furthermore, there is a significant difference in the way the N-terminal helical domain connects to the oligomerization core. In P22, the connection between these two domains is rigid (Figure 2B), while in a 4 Å structure of the SF6 full-length S-terminase (Büttner et al., 2012), no continuity is observed between N-termini and the oligomerization core (Figures 2E and 2F), suggesting a flexible hinge. The atomic structure of phage λ S-terminase (gpNu1) DNA-binding domain is also known (de Beer et al., 2002) (Figures 2G and 2H). This fragment (residues 1–68 of a 181-residue

protein) assembles into a dimer in solution and possesses a pair of winged helix-turn-helix DNA-binding motifs. λ -DNA-binding domain can be tentatively superimposed onto the P22 helical core with an rmsd ~ 3.6 Å (Figures S2B and S2C). This structural alignment is poor, however, and only 32 of the 68 residues of λ -DNA-binding domain superimpose onto P22 helices α_1 – α_3 . In addition, there is a topological inversion between the two polypeptide chains that point in opposite directions and P22 S-terminase lacks a wing, essential for DNA binding in winged helix-turn-helix DNA-binding motifs (Wintjens and Rooman, 1996). Finally, most of the residues in λ -DNA-binding domain directly involved in DNA binding (Lys5 in helix α_A and Arg17, Thr18, Gln20, Asn21, Gln23 in helix α_B) (de Beer et al., 2002) do not have a direct counterpart in P22. Finally, the structure of the T4-like phage 44RR S-terminase (gp16) (Figures 2I and 2J) also shows dramatic structural difference as compared to P22, to the point that structural superimposition was not attempted. Phage 44RR S-terminase is built by a simple α -helical hairpin and presents a significantly larger central channel (>35 Å in diameter depending on oligomeric state, 11 mers, or 12 mers) (Sun et al., 2012). Thus, viral S-terminase subunits differ dramatically in structure and oligomeric state, even within closely related phages that infect similar hosts. The lack of a winged helix-turn-helix DNA-binding motif in the N-terminus of P22

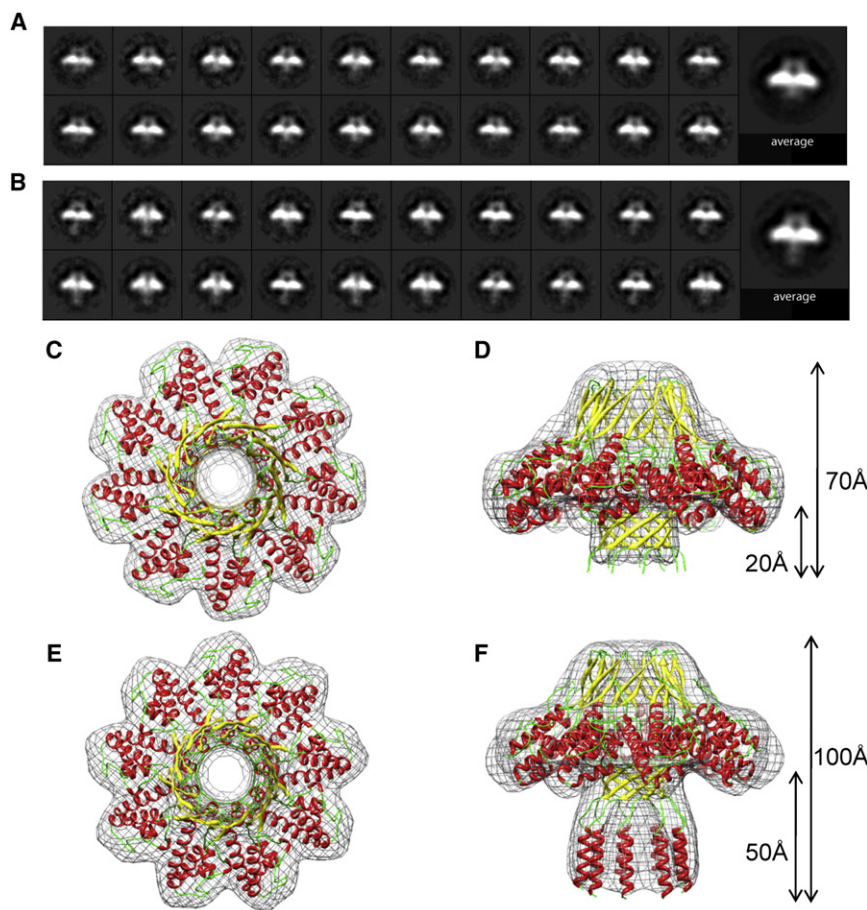


Figure 3. Single Particle Analysis of Negatively-Stained fl-S-Terminase Reveals Two Structurally Distinct Populations

(A and B) Class averages of full-length S-terminase reveal particles characterized by a short (A) and an extended barrel (B). Particles in (B) exhibit an extension of the DNA channel by ~ 30 Å as compared to particles in (A).

(C and D) A three-dimensional negative stain reconstruction (in gray) of S-terminase with a short barrel is overlaid to a ribbon model of the crystallographic structure of cleaved S-terminase spanning residues 1–139, shown in top (C) and side (D) views.

(E and F) Top (E) and side (F) views of a three-dimensional negative stain reconstruction of S-terminase particles with an extended barrel are overlaid to a model of the full-length S-terminase that includes the crystallographic structure and an hypothetical model of C-terminal residues 140–158 produced by Modeler (Sali and Blundell, 1993).

See also Figures S3F and S3G.

differences, a subset of 8,219 side-view particles from both populations underwent an additional round of alignment and classification. Whereas $\sim 80\%$ of the side-view particles exhibited a short barrel (Figure 3A), 20% of the particles presented an ~ 30 Å density extending outward from the nine-stranded β -barrel channel (referred to as extended barrel) (Figure 3B). The two differing populations of particles were separated into two

S-terminase suggests that this domain may not be directly involved in DNA binding.

S-Terminase C Terminus Is Partially Structured

Both in solution and in crystal, the C terminus of P22 S-terminase is highly susceptible to proteolysis (Roy et al., 2011). The amino acid sequence of residues 140–162 contains some of the signature features of intrinsically disordered proteins (Dyson and Wright, 2005), such as low sequence complexity and high amino-acid compositional bias (e.g., few bulky hydrophobic amino acids, high proportion of polar and charged amino acids like Arg, Glu, and Lys) (Figure S3A). However, unlike natively disordered proteins (Dyson and Wright, 2005), the residue sequence 142–156 (DRDKRRSRIKELFNR) has a high propensity to fold into a basic α helix (Figures S3B and SBE). These observations led us to hypothesize that the C terminus of S-terminase is structurally heterogeneous in solution, existing as an unstructured polypeptide chain in equilibrium with a folded α helix. To test this hypothesis, we analyzed particles of the full-length S-terminase subunit by negative-stain electron microscopy (EM) single particle analysis (Figure S3F). Reference-free alignment and classification of 22,665 automatically selected particles revealed the existence of two populations of S-terminase that appeared identical in top views, but had distinct features in side views. To perform a more detailed assessment of their

datasets and, together with top views, were used to compute a three-dimensional reconstruction of S-terminase in the two conformational states (Figures 3C–3F). The reconstruction of short-barrel S-terminase at 18 Å resolution (estimated by Fourier shell correlation at 0.5 criteria (Harauz and van Heel, 1986) (Figure S3G) fits well with the crystal structure of S-terminase lacking the DNA-binding domain (Figures 3C and 3D). Since the sample used for EM analysis was minimally degraded on SDS-PAGE, it is unlikely that this reconstruction corresponds exclusively to particles lacking C-terminal residues 140–162. Instead, the population of S-terminase with a short barrel represents particles with an unstructured C terminus, which by negative stained EM analysis is indistinguishable from cleaved S-terminase. In contrast, the population of S-terminase with an extended barrel (Figures 3E and 3F), also solved at 18 Å resolution (Figure S3G), fits well with a model of the full-length S-terminase that contains a structured C-terminal domain, with residues 142–156 possibly folded into a straight α helix (Figures S3C–S3E). In this hypothetical model, nine α helices assemble together to extend S-terminase barrel by ~ 30 Å (Figure 3F). Although at this resolution we cannot determine if the putative α helices lining the central channel are straight or bent with respect to the channel central axis, the fit between negative stain reconstruction and putative model of full-length S-terminase is remarkably good (Figure 3F). Interestingly, this model predicts that at least three basic side

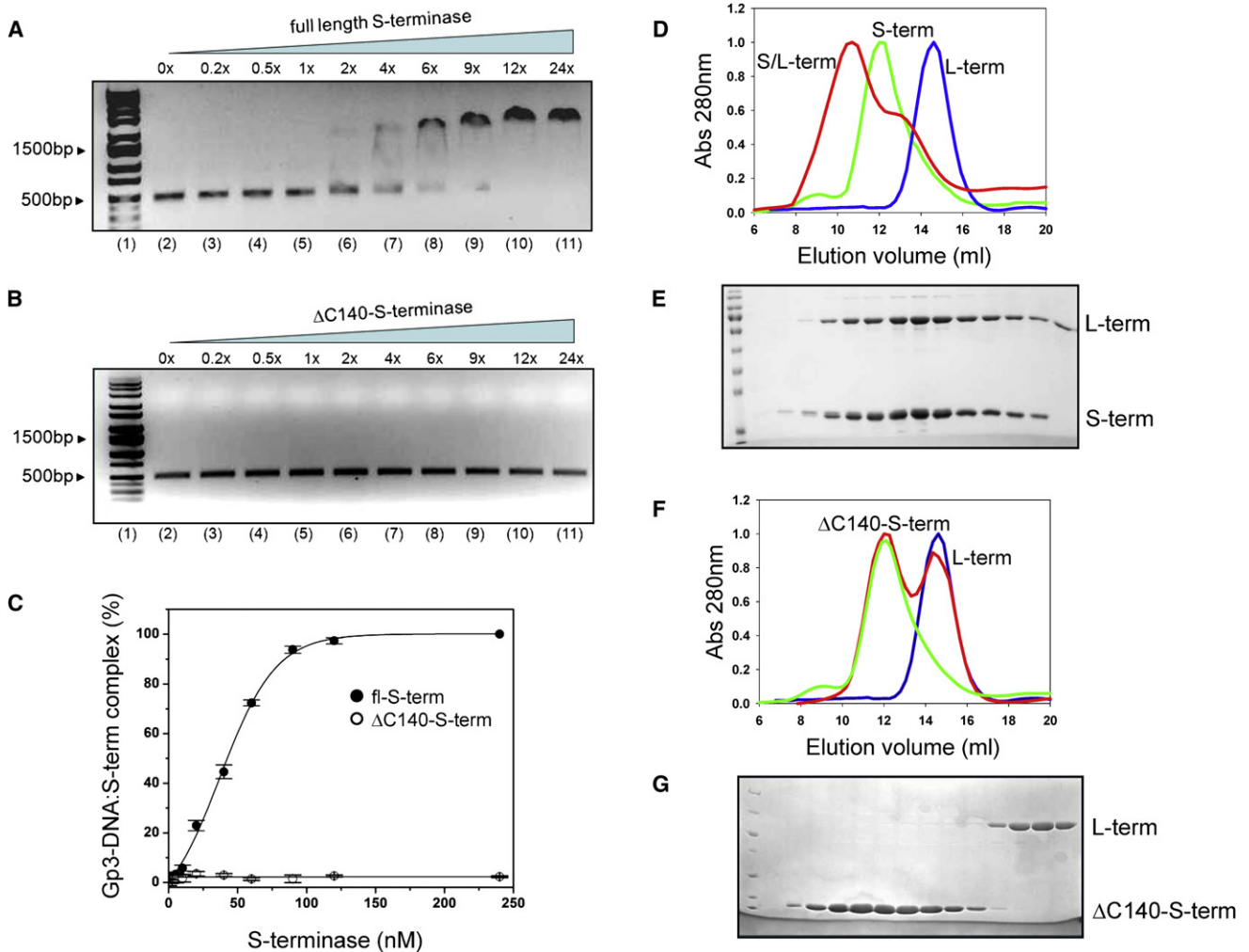


Figure 4. P22 S-Terminase DNA-Binding Activity

(A and B) EMSA of full-length S-terminase (A) or Δ C140-S-terminase (B) binding to gp3-DNA. In both panels, lanes 2–11 show a titration of 0- to 24-fold equivalents of fl- and Δ C140-S-terminase incubated with the gp3-DNA and separated on a 1.5% agarose gel followed by ethidium bromide staining.

(C) Quantification of EMSAs in (A,B) based on four independent repeats. Error bars are calculated from averaging the intensity of the gp3-DNA:S-terminase complex over four independent experiments.

(D and F) The binding of full-length S-terminase (D) or Δ C140-S-terminase (F) to L-terminase was characterized by SEC on a Superose 12 column; elution peaks for S-terminase, L-terminase and the S/L-terminase complex are shown in green, blue, and red, respectively.

(E and G) SDS-analysis of fractions eluted from gel filtration in panels (D) and (F), respectively.

chains (Lys146, Arg150, and Arg157) (Figures S3D and S3E) project into the central channel of each S-terminase, which would generate a highly basic inner core. Thus, single particle analysis of S-terminase particles supports the hypothesis of a plastic conformation of P22 S-terminase C terminus.

The C Terminus of P22 S-Terminase Mediates DNA-Binding and Formation of an Assembly Complex with L-Terminase

We used an electrophoretic mobility shift assay (EMSA) on agarose gel to investigate S-terminase DNA-binding activity. We PCR amplified P22 gene 3 (referred to as gp3-DNA), which contains a *pac* site between nucleotides 265–286 (Casjens et al., 1987; Casjens and King, 1974; Wu et al., 2002). Incubation

of full-length S-terminase with gp3-DNA (~500 bps) efficiently slowed down its electrophoretic mobility (Figure 4A). Quantification of this band-shift suggested a cooperative DNA-protein interaction (Figure 4C). Since the C terminus of P22 S-terminase is highly basic (Figure S3A), we tested its putative involvement in DNA binding. Strikingly, a deletion construct of S-terminase lacking residues 140–162, Δ C140-S-terminase, failed to bind gp3-DNA under identical experimental conditions (Figures 4B and 4C). To rule out the possibility that the C-terminal deletion had changed the oligomeric state of P22 S-terminase (as observed for bacteriophage SF6 (Büttner et al., 2012) and R44 (Sun et al., 2012) S-terminases) and its biochemical activity, we repeated the band-shift assay using cleaved S-terminase, obtained by limited proteolysis of full-length S-terminase with

chymotrypsin, which readily cleaves the last 23 residues (Roy et al., 2011). Proteolyzed S-terminase also showed complete loss of DNA binding (data not shown), confirming the results obtained with Δ C140-S-terminase.

To test if the nonameric S-terminase of bacteriophage P22 is competent for assembly to L-terminase, we performed binding studies using purified terminase subunits. By analytical size exclusion chromatography, S- and L-terminase migrated with elution volumes (E_{vol}) of \sim 12.1 and 15.1 ml (Figure 4D), corresponding to globular species of \sim 180 kDa (a nonamer) and 60 kDa (a monomer) (Nemecek et al., 2007), respectively. Incubating a 2-fold molar excess of L-terminase with S-terminase resulted in a larger species migrating with $E_{vol} \sim$ 10.1 ml, corresponding to \sim 300 kDa (Figure 4D). SDS-PAGE analysis (Figure 4E) confirmed that this species had both S- and L-terminase in approximate 3:2 molar ratio. Interestingly, Δ C140-S-terminase (or proteolytically cleaved S-terminase) incubated with L-terminase under identical experimental conditions failed to assemble into a complex (Figures 4F and 4G), yielding two distinct species migrating separately by SEC. Thus, the C terminus of P22 S-terminase is essential for DNA binding and assembly to L-terminase; deletion of C-terminal residues 140–162 (without altering the nonameric quaternary structure) results in complete loss of S-terminase function.

S-Terminase Is a DNA-Dependent ATPase-Activating Protein

To determine how S-terminase modulates the ATPase activity of L-terminase, we carried out an ATPase assay with radioactive $^{32}\gamma$ -ATP, using S- and L-terminase subunits, followed by thin layer chromatography on polyethyleneimine cellulose (PEI-TLC) (Figure 5A). Given the sensitivity of this radioactive assay, all factors used in the assay were $>$ 99% pure to avoid co-purification of contaminating ATPases from the expression host. At 37°C, in the absence of cold ATP (single-turnover ATPase assay), the intrinsic ATPase activity of L-terminase resulted in distinct release of $^{32}\text{P}_i$ that was \sim 18-fold greater than that caused by spontaneous hydrolysis of $^{32}\gamma$ -ATP in aqueous buffer (Figure 5A, lanes 2 and 1, respectively). The basal ATPase activity of L-terminase was reduced by \sim 10% in the presence of gp3-DNA (Figure 5A, lane 3). This small but reproducible drop in activity (Figure 5B) is likely due to the nuclease activity of L-terminase that generates free dNTPs, potentially competing with $^{32}\gamma$ -ATP for binding to L-terminase. Addition of nonameric S-terminase did not increase the ATPase activity of L-terminase in a statistically significant manner (Figure 5B, lane 4). While the intensity of released $^{32}\text{P}_i$ in Figure 5A, lane 4 appears greater than that in lane 2 (free L-terminase), this value has to be corrected for the $^{32}\text{P}_i$ released by free S-terminase in lane 8. As previously reported for at least three other S-terminases (gpNu1 in λ , gp16 in T4, and gp1 in SPP1; Rao and Feiss, 2008), ATPase activity was in fact observed for the full-length S-terminase of P22 (Figure 5A, lane 8), which lacks a classical Walker A- or Walker B-type ATP binding motif (Rao and Feiss, 2008). This full-length S-terminase ATPase activity was completely abolished by either adding gp3-DNA (Figure 5A, lane 9) or by cleaving off the DNA- and L-terminase binding domain (Figure 5A, lane 10). These data strongly suggest that P22 S-terminase is not a bona fide ATPase; the putative

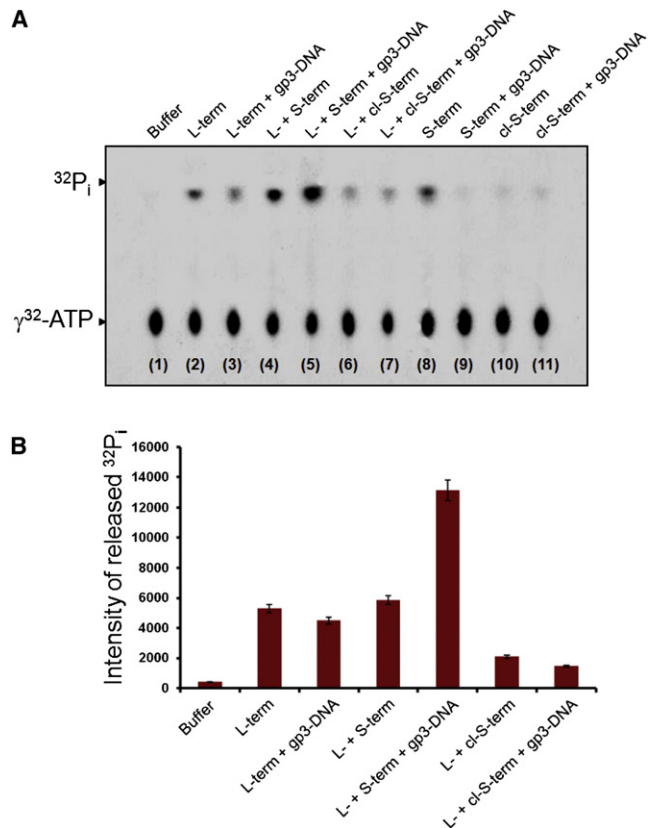


Figure 5. S-Terminase Activates the ATPase Activity of L-Terminase in the Presence of gp3-DNA

(A) ATPase assay resolved on PEI-TLC in the presence of different reactants and γ^{32} -ATP. The position of γ^{32} -ATP and $^{32}\text{P}_i$ is indicated by arrows (B). Quantification of $^{32}\text{P}_i$ released during the ATPase assay. The intensity of $^{32}\text{P}_i$ released by L-terminase in the presence of S-terminase and gp3-DNA (lanes 4–5 in Figure 5A) was corrected by subtracting the intensity of $^{32}\text{P}_i$ released in control reactions containing only S-terminase, with and without gp3-DNA (lanes 8–9 in Figure 5A). Error bars are calculated from averaging the intensity of $^{32}\text{P}_i$ released over five independent experiments carried out under identical conditions. The average standard deviation is usually less than 3%.

ATPase activity observed in vitro (Figure 5A, lane 8) likely results from the nonspecific binding of $^{32}\gamma$ -ATP to basic residues in the DNA-binding domain, which may facilitate its hydrolysis. Furthermore, since the addition of gp3-DNA dramatically reduced S-terminase ATPase activity (Figure 5A, lane 9), this rules out the possibility that the observed ATPase activity seen in our assay is due to contaminating ATPases, which, if present, would not be inhibited by DNA. In contrast, the ATPase activity of L-terminase was significantly stimulated by S-terminase in the presence of gp3-DNA (Figure 5A, lane 5). The synergistic action of L-terminase, S-terminase, and gp3-DNA enhanced $^{32}\text{P}_i$ release by \sim 42-fold as compared to spontaneous hydrolysis (Figure 5B). The ATPase activity of L-terminase in the presence of S-terminase and gp3-DNA was \sim 2.5-fold greater as compared to free L-terminase, and this effect was specifically and directly dependent on the presence of gp3-DNA (Figure 5B). Deletion of S-terminase DNA- and L-terminase binding domain reduced the ATPase activity of L-terminase by more than

10-fold (Figure 5B) both in the presence and absence of gp3-DNA (Figure 5A, lanes 7 and 6, respectively). Thus, P22 S-terminase bound to its own DNA functions as a specific ATPase-activating factor for L-terminase.

DISCUSSION

An open question in virology is how dsDNA bacteriophages and herpes viruses efficiently package their genomes into empty procapsids in the presence of a large excess (>100-fold) of host DNA. In a general transducing phage like P22, each round of infection results in only 2% of newly replicated particles that carry host DNA instead of the viral chromosome. Despite the large excess of host DNA present during packaging, the packaging reaction is robust and 98% of virions in vivo contain phage DNA (Ebel-Tsipis et al., 1972). This specificity implies the existence of a fine mechanism that allows P22 to discriminate, bind, and package its genome with greater affinity than host DNA. Likewise, to avoid wasteful hydrolysis of ATP when nonspecific DNA encounters the packaging motor, viruses must have developed fine mechanisms to regulate genome-packaging ATPase activity before and during the packaging reaction. To account for this regulation, both specific binding to packaging initiation sites and specific stimulation of genome-packaging ATPase activity have been ascribed to the S-terminase subunit that synergizes with L-terminase to sustain genome-packaging (Rao and Feiss, 2008).

The high resolution crystal structure of nonameric P22 S-terminase and the biochemical analysis presented in this study shed light on several unexpected properties governing the biology of viral S-terminases. First, there is a fundamental structural diversity among tailed bacteriophage S-terminase subunits, both at the level of protomer conformation and at the oligomer quaternary structure (Figure 2). P22 protomer is superimposable only to the closely related *Podoviridae* Sf6 albeit the latter forms octamers instead of nonamers. Intriguingly, the β -hairpin (β_1 - β_2) that forms the β -dome in P22, is absent in Sf6, but conserved in the SPP1-like phage SF6 (a *Siphoviridae*). This suggests that a complex shuffling of structural blocks must have occurred throughout evolution of tailed bacteriophages (Casjens and Thuman-Commike, 2011). The structural divergence of viral S-terminases is extreme between P22 and the T4-like phage 44RR (a *Myoviridae*), whose S-terminase subunit is completely different than in P22, both in fold (a helical hairpin) and in oligomerization state (11/12-mer versus 9-mer). Together with the structure, the functional mechanisms underlining DNA recognition are likely to have evolved and diverged throughout evolution, to the point that a universal mechanism for DNA binding is unlikely to exist. For instance, both P22 S-terminase and λ gpNu1 bind efficiently and cooperatively to DNA (de Beer et al., 2002). However, the N-terminal domain of P22 S-terminase does not contain a winged helix-turn-helix DNA-binding motif, as seen in λ gpNu1 (Figures S2B and S2C), and DNA recognition in P22 is fully dependent on C-terminal residues 140–162 (Figure 4). Interestingly, this moiety of P22 S-terminase is highly flexible and poorly structured both in solution (Roy et al., 2011) and in crystal, which suggests the DNA-binding domain may become preferentially stabilized upon binding to DNA as opposed to being constitu-

tively folded, as in λ . Deletion of C-terminal residues 140–162 completely abolishes both DNA- and L-terminase binding activity of P22 S-terminase (Figure 4). Since the structures of the full-length and cleaved S-terminase are identical, it is unlikely that the C-terminal deletion used in this study alters the three-dimensional conformation and/or oligomeric state and hence binding activity toward DNA and L-terminase. The location of a C-terminal DNA-binding domain in P22 S-terminase is consistent with the observation that deletion of residues 143–162 eliminates nonspecific DNA-binding activity (Nemecek et al., 2008). Finally, our finding of a C-terminal L-terminase-binding domain in P22 S-terminase agrees well with the recently proposed hypothesis by Casjens and Thuman-Commike that, based on evolutionary consideration, the C terminus of S-terminase mediates binding to L-terminase (Casjens and Thuman-Commike, 2011).

Eleven missense mutations that increase the frequency of phage P22 generalized transduction (high-frequency of transduction mutations) map to the gene encoding the S-terminase (Casjens et al., 1992). Intriguingly, only one out of eleven of these substitutions (Glu \rightarrow Lys)¹⁵² lies in the C terminus of S-terminase, which in P22 contains the DNA-binding domain. All other mutations mainly cluster in the center of the protein, within residues 80 and 112. This is unexpected, as, intuitively, one would expect mutations that increase efficiency of transduction to cluster in the putative DNA-binding domain. However, the high frequency of transduction phenotype is very complex and could be the resultant of completely indirect effects. For instance, the point mutation at position (Ala \rightarrow Val)¹¹² has been thought to increase the frequency of transduction by affecting the DNA-binding properties of S-terminase (Casjens et al., 1992). However, a similar mutation at the same position, (Ala \rightarrow Thr)¹¹² changes the oligomeric state of P22 S-terminase from nonamer to decamer (Nemecek et al., 2007) suggesting that the DNA-binding activity of S-terminase can be affected indirectly by point mutations that cause structural rearrangements in the oligomer conformation. Likewise, four of the eleven HT-mutations, (Leu \rightarrow Phe)⁸⁰, (Glu \rightarrow Lys)⁸¹, (Asp \rightarrow Asn)⁹¹, and (Val \rightarrow Ile)⁹⁵, are clustered at positions in close proximity to the *pac* site itself, which spans the region between codons 88 and 97 in gene 3 (Wu et al., 2002). This suggests that certain HT-missense mutations could affect the DNA recognition site more than the ability of S-terminase to recognize it.

Understanding the DNA- and L-terminase binding activity of P22 S-terminase led us to discover an unexpected property of this molecule. Upon binding to gp3-DNA, S-terminase becomes a specific activator of L-terminase ATPase activity. Both a construct of S-terminase lacking the DNA/L-terminase-binding domain (residues 140–162) and full-length S-terminase in the absence of gp3-DNA were unable to stimulate the ATPase activity of L-terminase (Figure 5), thus confirming that specific binding to DNA is required to stimulate genome packaging. The role of DNA in this interaction may involve wide conformational stabilization of S-terminase that folds a C-terminal domain, thus igniting the packaging engine to fire ATP hydrolysis. This, in turn, could lower the entropic barrier of inserting the linear end of the P22 genome into the procapsid, thus triggering the packaging reaction in the same manner as a spark ignites a combustion-engine.

How is viral DNA recognized by S-terminase? It was previously proposed that S-terminases may recognize viral DNA using a nucleosome-like recognition characterized by wrapping dsDNA around the outer rim of the S-terminase ring formed by its N-terminus domains (Büttner et al., 2012; de Beer et al., 2002; Nemecek et al., 2008; Sun et al., 2012; Zhao et al., 2010). This model has quickly gained popularity in the literature, although it lacks experimental validation. The structural and biochemical results presented in this work do not support this model. In the absence of a strong, biochemically detectable DNA-binding activity in the N-terminal domain, it would be energetically too costly to bend dsDNA around this domain. In addition, the nucleosome-like model does not assign a function to the central ~23 Å diameter channel in P22 S-terminase that is large enough to accommodate hydrated dsDNA (Vlieghe et al., 1999). Our discovery of a C-terminal DNA-binding site makes it plausible to speculate that DNA could be threaded through the internal channel as in a portal protein (Olia et al., 2011) as opposed to being wrapped on the outside of S-terminase like a gear, although other assembly models are certainly possible and cannot be ruled out a priori without experimental validation.

In conclusion, the structural diversity of viral S-terminase subunits, the lack of a unique quaternary structure oligomeric state, and the fundamentally different way by which viruses package DNA lend support to the idea that S-terminases recognize viral genomes differently, and a universal mechanism for DNA binding is not likely to exist. Whatever mechanism P22 S-terminase uses to recruit gp3-DNA, this work demonstrates that DNA- and L-terminase binding activities require the protein C terminus and DNA binding is coupled to stimulation of L-terminase ATPase activity, which triggers ATP-dependent genome packaging.

EXPERIMENTAL PROCEDURES

Molecular Biology Techniques

The genes encoding small (gp3) and large (gp2) terminase subunits were PCR amplified from P22 genomic DNA (Pedulla et al., 2003) and ligated between BamHI and HindIII restriction sites of expression vectors pMal-2cE (New England Biolabs) and pET-28a (Novagen), respectively. The mutant Δ C140-S-terminase was constructed by introducing a stop codon at position 140 of S-terminase. All plasmids were sequenced to confirm the fidelity of the DNA sequence. Expression and purification of full-length and Δ C140-S-terminase and limited proteolysis of full-length S-terminase with chymotrypsin to obtain cleaved S-terminase (residues 1–139) was carried out as described (Roy et al., 2011). L-terminase was also expressed in *E. coli* strain BL21 (DE3/pLysS) by induction at 16°C for 16 hr with 0.5 mM isopropyl- β -D-1-thiogalactopyranoside. Cell pellets expressing L-terminase were lysed by sonication in Lysis Buffer (20 mM Tris-HCl, pH 7.5, 300 mM NaCl, 0.1% (v/v) CHAPS (3-[(3-Cholamidopropyl)dimethylammonio]-1-propanesulfonate), 5 mM β -Mercaptoethanol, 1 mM PMSF). L-terminase was purified by Ni²⁺ affinity chromatography followed by size-exclusion chromatography on a Superdex 200 column (GE Life Sciences) equilibrated in 20 mM Tris-HCl, 150 mM NaCl, 5 mM β -Mercaptoethanol, 5% (v/v) glycerol, pH 7.5.

Structure Determination

Crystallization of cleaved S-terminase was previously described (Roy et al., 2011). The best crystals were obtained at pH 7.0 using 20% (w/v) PEG 3350 in the presence of 0.2 M potassium thiocyanate. Expression of semet-derivatized S-terminase was carried out as described by Olia et al. (Olia et al., 2011). Purification of semet-derivatized S-terminase was identical to that of the wild-type protein (Roy et al., 2011). The structure was solved by single-wavelength anomalous dispersion using a single semet-derivatized crystal at

the National Synchrotron Light Source beam-line X6A at a wavelength of 0.976 Å (Table 1). The positions of 27 selenium sites (3 per subunit) were located using Phenix (Adams et al., 2002). Initial phases to 2.5 Å resolution were improved by 9-fold noncrystallographic symmetry-averaging and extended to the resolution of the native data (1.75 Å). A partial model was built by Autobuild, in Phenix (Adams et al., 2002), and completed manually in Coot (Emsley and Cowtan, 2004). The structure was then subjected to seven cycles of positional and anisotropic B-factor refinement in Phenix (Adams et al., 2002). To lower the R_{free} below 29%, noncrystallographic symmetry restraints were not used during refinement. Peaks above 3σ in a $F_o - F_c$ difference electron density map were modeled as water molecules. The structure of P22 S-terminase has been refined to a $R_{\text{work}}/R_{\text{free}}$ of 17.73/21.65%, at 1.75 Å resolution. The final S-terminase model contains residues 1–139 for chain A, 5–139 for chain D, 6–139 for chain F, 7–139 for chains C and G, and 8–139 for chains B, E, H, and I, respectively. The final model also contains 1,397 water molecules. The model has excellent geometry (Table 1), with 100% residues in the most favored regions of the Ramachandran plot, and a root mean square deviation (rmsd) of bond lengths and angles of 0.006 Å and 0.918°, respectively. All Ribbon models were generated using PyMol (DeLano, 2002) or Chimera (Pettersen et al., 2004). Crystallization and structure determination of full-length S-terminase are described in Supplementary Information.

Negative Stain Electron Microscopy and Single Particle Analysis

Full-length nonameric S-terminase at a concentration of ~2 μ M were applied to glow discharged carbon coated copper grids and negatively stained with 2% phosphotungstic acid, as previously described (Nemecek et al., 2007). Electron micrographs were automatically acquired on a Tecnai F20 transmission electron microscope operating at 120 keV using Legikon data collection software (Suloway et al., 2005). Micrographs were collected on a Tietz F415 CCD camera at a nominal magnification of 50,000 \times (1.63 Å/pixel) with an underfocus range of 0.7 to 1.5 microns. All processing was performed within the Appion software package (Lander et al., 2009). From an initial dataset of 88,147 automatically selected particles, a subset of 22,665 properly centered particles that did not have closely neighboring densities were extracted for image processing. The particles were aligned and classified to generate two-dimensional class averages in a reference-independent method using the IMAGIC image processing software (van Heel et al., 1996). Side-view particles were separated from top-view particles, and the side-view particles were further classified into short- and extended-barrel datasets. The initial references for the three-dimensional reconstructions were generated by angular reconstitution of the class averages while imposing c_9 symmetry. The three-dimensional models were improved by refinement of the particles against the model over the course of 20 iterations using the EMAN2 software package (Tang et al., 2007). The reported resolutions of the reconstructions according to Fourier shell correlation at 0.5 (Harauz and van Heel, 1986) are 18.1 and 18.2 for the short- and extended-barrel structures, respectively (Figure S3). The negative stain reconstructions were visualized using the program Chimera (Pettersen et al., 2004). X-ray structures were fit in the reconstructions manually and then the fit was improved using the command “Fit Models in Maps” in Chimera (Pettersen et al., 2004).

EMSA, SEC, and ATPase Assay

DNA fragments corresponding to the coding region of P22 gene 3 (486 bp) were amplified by PCR from a P22 genomic DNA and purified by gel extraction. EMSAs were carried out by adding 0 to 24 molar equivalents of nonameric S-terminase (corresponding to 0–240 nM) to gp3-DNA (at a fixed concentration of 10 nM) in a 50 μ l reaction volume, containing 50 mM NaCl, 1 mM EDTA, 10 mM Tris-HCl pH 7.5. Samples were incubated at room temperature for 30 min and then electrophoresed in a 1.5% (w/v) agarose gel with 1 X TAE (Tris-Acetate-EDTA) buffer at 100 V for approximately 45 min, followed by ethidium bromide staining. Bands corresponding to the S-terminase:DNA complex were quantified using ImageJ (Abramoff et al., 2004), and the percentage of the complex was plotted against the known concentration of S-terminase using the program Origin. Analytical size-exclusion chromatography (SEC) analysis was carried out on a Superose 12 column (G.E. Healthcare) pre-equilibrated in 10 mM Tris, pH 8.0, 150 mM NaCl and 5 mM β -Mercaptoethanol as described (Pumroy et al., 2012) (Supplementary Information). The ATPase-stimulating activity of S-terminase was measured using

a radioactive ATPase assay as described by Leffers and Rao (Leffers and Rao, 2000). All factors used in this assay were > 99% pure as judged by sodium dodecyl sulfate polyacrylamide gel electrophoresis (SDS-PAGE) and matrix-assisted laser desorption/ionization (MALDI) mass spectrometry analysis. Purified L-terminase (1 μ M) was incubated with 5 μ M purified S-terminase (e.g., full-length Sterminase or cleaved S-terminase) in the presence of 75 nM [γ - 32 P]ATP (specific activity, 3000 Ci/mmol; PerkinElmer, Inc.) in ATPase buffer (50 mM Tris-HCl, pH 7.5, 0.1 M NaCl, 5 mM MgCl₂). To test if DNA enhances S-terminase ATPase-activating activity, 20 nM gp3-DNA (corresponding to one copy of gp3-DNA per ~20 equivalents of nonameric S-terminase) or nonspecific DNA (empty pUC19 vector) was added to the reaction mixture. Control experiments included free S-terminase with or without gp3-DNA. The total reaction volume was set to 20 μ l and samples were incubated for 20 min at 37°C. Reactions were terminated by adding EDTA to 50 mM final concentration and 1 μ l reaction mixture was spotted on a TLC-PEI plate (Sigma-Aldrich). TLC plates were developed (Leffers and Rao, 2000), air-dried, autoradiographed and the intensity of each spot quantified using ImageJ (Abramoff et al., 2004). The intensity of 32 P_i released by L-terminase in the presence of S-terminase was determined by subtracting the amount of 32 P_i released by free S-terminase incubated with [γ - 32 P]ATP under identical conditions.

ACCESSION NUMBERS

The coordinates and structure factors for the high resolution structure of S-terminase have been deposited in the Protein Data Bank under ID code 3P9A.

SUPPLEMENTAL INFORMATION

Supplemental Information includes three figures, Supplemental Experimental Procedures, and Supplemental References and can be found with this article online at <http://dx.doi.org/10.1016/j.str.2012.05.014>.

ACKNOWLEDGMENTS

We are grateful to Vivian Stojanoff at the NSLS and to the macCHESS staff for beam time and assistance in data collection. We thank David Price at the University of Iowa for useful suggestions on the ATPase assay. Electron microscopic imaging and reconstruction were conducted at the National Resource for Automated Molecular Microscopy, which is supported by the NIH through a P41 program grant (RR17573) from the National Center for Research Resources. This work was supported by NIH Grants 1R56 AI095974-01 and 1R01GM100888-01A1 to G.C.

Received: March 25, 2012

Revised: April 30, 2012

Accepted: May 19, 2012

Published online: July 5, 2012

REFERENCES

- Abramoff, M.D., Magelhaes, P.J., and Ram, S.J. (2004). Image processing with ImageJ. *Biophotonics International* 11, 36–42.
- Ackermann, H.W. (2003). Bacteriophage observations and evolution. *Res. Microbiol.* 154, 245–251.
- Adams, P.D., Grosse-Kunstleve, R.W., Hung, L.W., Ioerger, T.R., McCoy, A.J., Moriarty, N.W., Read, R.J., Sacchettini, J.C., Sauter, N.K., and Terwilliger, T.C. (2002). PHENIX: building new software for automated crystallographic structure determination. *Acta Crystallogr. D Biol. Crystallogr.* 58, 1948–1954.
- Baumann, R.G., and Black, L.W. (2003). Isolation and characterization of T4 bacteriophage gp17 terminase, a large subunit multimer with enhanced ATPase activity. *J. Biol. Chem.* 278, 4618–4627.
- Büttner, C.R., Chechik, M., Ortiz-Lombardía, M., Smits, C., Ebong, I.O., Chechik, V., Jeschke, G., Dykeman, E., Benini, S., Robinson, C.V., et al. (2012). Structural basis for DNA recognition and loading into a viral packaging motor. *Proc. Natl. Acad. Sci. USA* 109, 811–816.
- Camacho, A.G., Gual, A., Lurz, R., Tavares, P., and Alonso, J.C. (2003). Bacillus subtilis bacteriophage SPP1 DNA packaging motor requires terminase and portal proteins. *J. Biol. Chem.* 278, 23251–23259.
- Casjens, S., and King, J. (1974). P22 morphogenesis. I: Catalytic scaffolding protein in capsid assembly. *J. Supramol. Struct.* 2, 202–224.
- Casjens, S., Huang, W.M., Hayden, M., and Parr, R. (1987). Initiation of bacteriophage P22 DNA packaging series. Analysis of a mutant that alters the DNA target specificity of the packaging apparatus. *J. Mol. Biol.* 194, 411–422.
- Casjens, S., Sampson, L., Randall, S., Eppler, K., Wu, H., Petri, J.B., and Schmiegler, H. (1992). Molecular genetic analysis of bacteriophage P22 gene 3 product, a protein involved in the initiation of headful DNA packaging. *J. Mol. Biol.* 227, 1086–1099.
- Casjens, S.R. (2011). The DNA-packaging nanomotor of tailed bacteriophages. *Nat. Rev. Microbiol.* 9, 647–657.
- Casjens, S.R., and Thuman-Commike, P.A. (2011). Evolution of mosaic-related tailed bacteriophage genomes seen through the lens of phage P22 virion assembly. *Virology* 411, 393–415.
- Catalano, C.E., ed. (2005). *Viral Genome Packaging Machines: Genetics, Structure and Mechanism* (New York: Springer), pp. 1–4.
- Cingolani, G., Moore, S.D., Prevelige, P.E., Jr., and Johnson, J.E. (2002). Preliminary crystallographic analysis of the bacteriophage P22 portal protein. *J. Struct. Biol.* 139, 46–54.
- de Beer, T., Fang, J., Ortega, M., Yang, Q., Maes, L., Duffy, C., Berton, N., Sippy, J., Overduin, M., Feiss, M., and Catalano, C.E. (2002). Insights into specific DNA recognition during the assembly of a viral genome packaging machine. *Mol. Cell* 9, 981–991.
- DeLano, W.L. (2002). <http://www.pymol.org>.
- Duffy, C., and Feiss, M. (2002). The large subunit of bacteriophage lambda's terminase plays a role in DNA translocation and packaging termination. *J. Mol. Biol.* 316, 547–561.
- Dyson, H.J., and Wright, P.E. (2005). Intrinsically unstructured proteins and their functions. *Nat. Rev. Mol. Cell Biol.* 6, 197–208.
- Ebel-Tsipis, J., Botstein, D., and Fox, M.S. (1972). Generalized transduction by phage P22 in Salmonella typhimurium. I. Molecular origin of transducing DNA. *J. Mol. Biol.* 71, 433–448.
- Emsley, P., and Cowtan, K. (2004). Coot: model-building tools for molecular graphics. *Acta Crystallogr. D Biol. Crystallogr.* 60, 2126–2132.
- Fuller, D.N., Raymer, D.M., Kottadiel, V.I., Rao, V.B., and Smith, D.E. (2007). Single phage T4 DNA packaging motors exhibit large force generation, high velocity, and dynamic variability. *Proc. Natl. Acad. Sci. USA* 104, 16868–16873.
- Galdiero, S., Galdiero, M., and Pedone, C. (2007). beta-Barrel membrane bacterial proteins: structure, function, assembly and interaction with lipids. *Curr. Protein Pept. Sci.* 8, 63–82.
- Harauz, G., and van Heel, M. (1986). Exact filters for general geometry three dimensional reconstruction. *Optik (Stuttg.)* 73, 146–156.
- Heinig, M., and Frishman, D. (2004). STRIDE: a web server for secondary structure assignment from known atomic coordinates of proteins. *Nucleic Acids Res.* 32 (Web Server issue), W500–502.
- Jackson, E.N., Jackson, D.A., and Deans, R.J. (1978). EcoRI analysis of bacteriophage P22 DNA packaging. *J. Mol. Biol.* 118, 365–388.
- Kanamaru, S., Kondabagil, K., Rossmann, M.G., and Rao, V.B. (2004). The functional domains of bacteriophage t4 terminase. *J. Biol. Chem.* 279, 40795–40801.
- Lander, G.C., Stagg, S.M., Voss, N.R., Cheng, A., Fellmann, D., Pulokas, J., Yoshioka, C., Irving, C., Mulder, A., Lau, P.W., et al. (2009). Appion: an integrated, database-driven pipeline to facilitate EM image processing. *J. Struct. Biol.* 166, 95–102.
- Leffers, G., and Rao, V.B. (2000). Biochemical characterization of an ATPase activity associated with the large packaging subunit gp17 from bacteriophage T4. *J. Biol. Chem.* 275, 37127–37136.

- Lin, H., Simon, M.N., and Black, L.W. (1997). Purification and characterization of the small subunit of phage T4 terminase, gp16, required for DNA packaging. *J. Biol. Chem.* *272*, 3495–3501.
- Lorenzen, K., Olia, A.S., Uetrecht, C., Cingolani, G., and Heck, A.J. (2008). Determination of stoichiometry and conformational changes in the first step of the P22 tail assembly. *J. Mol. Biol.* *379*, 385–396.
- Maluf, N.K., Gaussier, H., Bogner, E., Feiss, M., and Catalano, C.E. (2006). Assembly of bacteriophage lambda terminase into a viral DNA maturation and packaging machine. *Biochemistry* *45*, 15259–15268.
- Nadal, M., Mas, P.J., Blanco, A.G., Aman, C., Solà, M., Hart, D.J., and Coll, M. (2010). Structure and inhibition of herpesvirus DNA packaging terminase nuclease domain. *Proc. Natl. Acad. Sci. USA* *107*, 16078–16083.
- Nemecek, D., Gilcrease, E.B., Kang, S., Prevelige, P.E., Jr., Casjens, S., and Thomas, G.J., Jr. (2007). Subunit conformations and assembly states of a DNA-translocating motor: the terminase of bacteriophage P22. *J. Mol. Biol.* *374*, 817–836.
- Nemecek, D., Lander, G.C., Johnson, J.E., Casjens, S.R., and Thomas, G.J., Jr. (2008). Assembly architecture and DNA binding of the bacteriophage P22 terminase small subunit. *J. Mol. Biol.* *383*, 494–501.
- Olia, A.S., Prevelige, P.E., Jr., Johnson, J.E., and Cingolani, G. (2011). Three-dimensional structure of a viral genome-delivery portal vertex. *Nat. Struct. Mol. Biol.* *18*, 597–603.
- Pedula, M.L., Ford, M.E., Karthikeyan, T., Houtz, J.M., Hendrix, R.W., Hatfull, G.F., Poteete, A.R., Gilcrease, E.B., Winn-Stapley, D.A., and Casjens, S.R. (2003). Corrected sequence of the bacteriophage p22 genome. *J. Bacteriol.* *185*, 1475–1477.
- Pettersen, E.F., Goddard, T.D., Huang, C.C., Couch, G.S., Greenblatt, D.M., Meng, E.C., and Ferrin, T.E. (2004). UCSF Chimera—a visualization system for exploratory research and analysis. *J. Comput. Chem.* *25*, 1605–1612.
- Pumroy, R.A., Nardozi, J.D., Hart, D.J., Root, M.J., and Cingolani, G. (2012). Nucleoporin Nup50 stabilizes closed conformation of armadillo repeat 10 in importin α 5. *J. Biol. Chem.* *287*, 2022–2031.
- Rao, V.B., and Feiss, M. (2008). The bacteriophage DNA packaging motor. *Annu. Rev. Genet.* *42*, 647–681.
- Roy, A., and Cingolani, G. (2012). Structure of P22 headful packaging nuclease. *J. Biol. Chem.* Published online June 18, 2012. <http://dx.doi.org/10.1074/jbc.M112.349894>.
- Roy, A., Bhardwaj, A., and Cingolani, G. (2011). Crystallization of the nonameric small terminase subunit of bacteriophage P22. *Acta Crystallogr. Sect. F Struct. Biol. Cryst. Commun.* *67*, 104–110.
- Sali, A., and Blundell, T.L. (1993). Comparative protein modelling by satisfaction of spatial restraints. *J. Mol. Biol.* *234*, 779–815.
- Smits, C., Chechik, M., Kovalevskiy, O.V., Shevtsov, M.B., Foster, A.W., Alonso, J.C., and Antson, A.A. (2009). Structural basis for the nuclease activity of a bacteriophage large terminase. *EMBO Rep.* *10*, 592–598.
- Suloway, C., Pulokas, J., Fellmann, D., Cheng, A., Guerra, F., Quispe, J., Stagg, S., Potter, C.S., and Carragher, B. (2005). Automated molecular microscopy: the new Legimon system. *J. Struct. Biol.* *151*, 41–60.
- Sun, S., Kondabagil, K., Gentz, P.M., Rossmann, M.G., and Rao, V.B. (2007). The structure of the ATPase that powers DNA packaging into bacteriophage T4 procapsids. *Mol. Cell* *25*, 943–949.
- Sun, S., Kondabagil, K., Draper, B., Alam, T.I., Bowman, V.D., Zhang, Z., Hegde, S., Fokine, A., Rossmann, M.G., and Rao, V.B. (2008). The structure of the phage T4 DNA packaging motor suggests a mechanism dependent on electrostatic forces. *Cell* *135*, 1251–1262.
- Sun, S., Rao, V.B., and Rossmann, M.G. (2010). Genome packaging in viruses. *Curr. Opin. Struct. Biol.* *20*, 114–120.
- Sun, S., Gao, S., Kondabagil, K., Xiang, Y., Rossmann, M.G., and Rao, V.B. (2012). Structure and function of the small terminase component of the DNA packaging machine in T4-like bacteriophages. *Proc. Natl. Acad. Sci. USA* *109*, 817–822.
- Tang, G., Peng, L., Baldwin, P.R., Mann, D.S., Jiang, W., Rees, I., and Ludtke, S.J. (2007). EMAN2: an extensible image processing suite for electron microscopy. *J. Struct. Biol.* *157*, 38–46.
- van Heel, M., Harauz, G., Orlova, E.V., Schmidt, R., and Schatz, M. (1996). A new generation of the IMAGiC image processing system. *J. Struct. Biol.* *116*, 17–24.
- Vlieghe, D., Turkenburg, J.P., and Van Meervelt, L. (1999). B-DNA at atomic resolution reveals extended hydration patterns. *Acta Crystallogr. D Biol. Crystallogr.* *55*, 1495–1502.
- White, J.H., and Richardson, C.C. (1987). Gene 18 protein of bacteriophage T7. Overproduction, purification, and characterization. *J. Biol. Chem.* *262*, 8845–8850.
- Wintjens, R., and Rooman, M. (1996). Structural classification of HTH DNA-binding domains and protein-DNA interaction modes. *J. Mol. Biol.* *262*, 294–313.
- Wu, H., Sampson, L., Parr, R., and Casjens, S. (2002). The DNA site utilized by bacteriophage P22 for initiation of DNA packaging. *Mol. Microbiol.* *45*, 1631–1646.
- Zhao, H., Finch, C.J., Sequeira, R.D., Johnson, B.A., Johnson, J.E., Casjens, S.R., and Tang, L. (2010). Crystal structure of the DNA-recognition component of the bacterial virus Sf6 genome-packaging machine. *Proc. Natl. Acad. Sci. USA* *107*, 1971–1976.